Poiseuille and Nusselt Numbers for Laminar Flow in Microchannels with Rounded Corners

Marco LORENZINI[1,*] , Gian Luca MORINI[1],

* Corresponding author: Tel.: ++39 051 2093293; Fax: ++39 051 2090544; Email: marco.lorenzini@unibo.it
1: DIENCA Alma Mater Studiorum - Università di Bologna, I

Abstract This work investigates the frictional and heat transfer behaviour of laminar, fully-developed flow in microchannels with trapezoidal and rectangular cross-section and rounded corners under H1 boundary conditions. The equations of momentum and energy are solved numerically, and the results validated with analytical data, when available. The runs have been carried out for different aspect ratios and nondimensional radii of curvature R_c, with either all sides or three sides heated, one short side adiabatic for rectangular geometries and three sides heated, the longest one adiabatic for trapezoidal geometries. The Poiseuille and Nusselt numbers are reported and show, for the rectangular cross-section heated on all sides, a maximum increase for the highest value of the aspect ratio (β=1) with increments in the Poiseuille and Nusselt numbers of about 11% and 16% respectively for values of R_c^* of 0.5, increasing as the geometry approaches the circular duct (12.5% and 21%). The increase is less pronounced as β decreases and also when only three sides are heated (maximum increase of Nu around 10%); in the case of the trapezoidal geometry the effects of rounding the corners are almost negligible (a maximum increase in Nu of around 2%).

Keywords: Laminar Flow, Microchannel, Nusselt Number, Poiseuille number.

1. Introduction

Microsystems have enjoyed an ever-increasing development in the past two decades, which has spurred research aimed at understanding the basic phenomena that govern heat transfer and fluid flow in microchannels, which represent the building block of all micro-flow devices (MFDs). The knowledge gained so far has been summarized in several review works, e.g. a general survey of experimental results for convective flows in microchannels by Morini, 2004, or a recent one on liquid flows in microchannels by Collins et al., 2008. In spite of intensive research and several publications on the subject, some aspects remain uninvestigated, among which is the case of microchannels with rounded corners. In the last years an effort has been made in order to use standard semiconductor processes for the realization of different kinds of unconventional (channels of various shapes, sharp convex and rounded concave corner structures, etc) silicon structures for MEMS-based devices as highlighted recently by Pal and Sato, 2009. In micro-flow devices in which convective heat transfer occurs the analysis of the role of channel shape on the operative performance of the devices can give important feedback even on the optimization of the micro-fabrication process. For example, smoothing of corners and edges may result from fabrication procedures, a low degree of undercutting (i.e. high radii of curvature) are regarded unfavorably from the mechanical point of view, but they can have enhancing effects in terms of heat transfer, as shall be demonstrated in the following, with an increase in the frictional characteristics less pronounced: this makes rounding an interesting option, if no mechanical constraints bar it. This work aims at determining the frictional and heat transfer characteristics of laminar, fully-developed flows under H1 boundary conditions in microchannels of rectangular and trapezoidal potassium hydroxide(KOH)-etched cross-section with rounded corners for different values of the aspect ratio and of the radius of curvature. Results are presented in non-dimensional form

and compared to those available in the literature for the cases available (Shah and London, 1978, Morini and Spiga, 2007), and correlations are given expressing the values of the Poiseuille and Nusselt numbers as a function of the nondimensional radius of curvature.

2. Geometries investigated

The base geometries to be tested are those referring to microchannels of rectangular and trapezoidal KOH-etched cross-section, as depicted in Fig. 1.

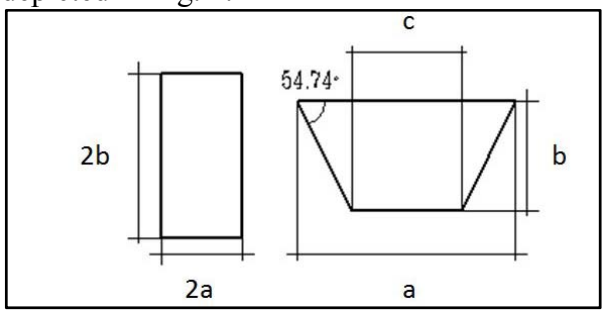

Figure 1 – Rectangular and trapezoidal cross-sections.

Starting from these configurations, progressive rounding of the corners is introduced through the increase of radius of curvature, R_c. (R_c=0 corresponding to sharp corners) In the former case, the aspect ratio is defined as

$$\beta=\frac{2a}{2b} \qquad (1)$$

thus, $\beta\leq 1$, and the radius of curvature is bounded by half the length of the shorter side (in order to avoid sharp junctions with the straight sides), $R_c\leq a$, which also implies

$$R_c^*=\frac{R_c}{b}\leq\beta \qquad (2)$$

The maximum achievable radius of curvature, in the case of a square duct (β=1), thus yields a circular cross-section. The characteristic dimension for the geometries investigated is the hydraulic diameter, which, for the rectangular cross-section with sharp corners has the following expression:

$$D_h = 2a\cdot\frac{2}{(1+\beta)} \qquad (3)$$

and is modified suitably in the case of rounded sections using the definition of D_h as 4A/P, where A is the cross-sectional area and P the corresponding wetted perimeter.

In the case of trapezoidal microchannels, which are normally obtained through chemical etching of <110> silicon wafers, the expression for the hydraulic diameter is slightly more involved. If φ is the angle between sides a and b of Fig. 1, one gets

$$D_h=b\cdot 2\beta\,\frac{1+\frac{\beta}{\tan\varphi}}{1+\beta\left(\frac{1}{\tan\varphi}+\frac{1}{\sin\varphi}\right)} \qquad (4)$$

for the case of sharp corners, which is again modified when $R_c\neq 0$ using the definition of hydraulic diameter.

In the case of trapezoidal cross-sections, β is defined as (Morini and Spiga, 2007):

$$\beta=\frac{c}{b} \qquad (5)$$

It is to be remarked that, with this definition, there is no upper bound to the value of β, as β goes to infinity the cross-section degenerates into a triangle.

Side a is the one from which etching starts, and can be sealed with a different, insulating material: a realization of a microchannel heat sink under the aforementioned conditions is shown in Fig. 2.

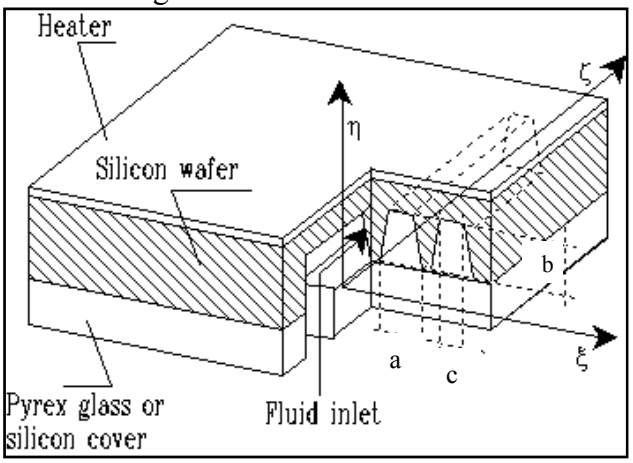

Figure 2 – Heat sink with trapezoidal microchannels.

As a consequence of the manufacturing process, it is the bottom side, b, whose corners can be smoothed with a given radius of curvature, R_c. In the simulations the radius of curvature has been constrained by the dimensions of c and b, in order to avoid cusps at the connections with the sides. It is expedient to define a non dimensional parameter, γ, such that

$$\gamma=\frac{R_c}{c} \qquad (6)$$

when c<0.5b (smooth connection between rounded corner and slanted side), and

$$\gamma=\frac{2R_c}{b} \qquad (7)$$

when c≥0.5b (to avoid the two rounded corners to intersect and crate a cusp at midpoint of side b). The advantage of this definition of γ is that in both cases:

$$0\leq\gamma\leq1 \qquad (8)$$

2. Mathematical model

Let us consider the silicon microchannel heat sink shown in Fig. 2; the microchannels obtained by chemical etching on the silicon wafer are in general closed by a Pyrex glass cover bonded to the substrate or by means of a silicon wafer. A liquid flows through the channels; due to the small size of the microchannels the flow is typically laminar. The microchannels have an axially unchanging cross-section with area equal to Ω and a wetted perimeter equal to Γ. A Cartesian system of coordinates ξ, η, ζ is assumed, with its origin in the left bottom corner of the inlet cross-section.

If a fixed linear power q_{wall} is imposed on the top of the silicon substrate while all the other outer walls of the unit cell are adiabatic, it may be reasonably assumed that the channels can be studied as long ducts subject to H1 boundary conditions, either with all sides heated or one side adiabatic (Morini and Spiga 2007); this analysis is far less cost-intensive in terms of computational time as compared to a full 3-D conjugate study without losing in detail. Some simplifying assumptions can be made before using the conventional Navier-Stokes and energy equations to compute the velocity and temperature distribution. The major assumptions for this work can be summarized as follows:

1. The fluid is Newtonian, incompressible, and with a laminar fully developed profile of velocity u(ξ,η) and a uniform inlet temperature θ_{in}.
2. The transport processes are considered to be steady-state and bi-dimensional (through the microchannel the velocity and the temperature profiles are considered as fully developed).
3. All the channel walls are rigid and nonporous.
4. Thermal radiation is neglected.
5. Axial thermal conduction (Pe>>1), natural convection (Gr/Re^2<<1), and interior heat sources are neglected.
6. Solid and fluid thermophysical properties are assumed to be constant with temperature.
7. The influence of viscous dissipation can be neglected.

Under the aforementioned hypotheses the conservation equations for momentum and energy take the form:

$$\nabla^2 u=\frac{1}{\mu}\frac{dp}{d\zeta} \qquad (9)$$

$$\nabla^2\vartheta=\frac{u(\xi,\eta)}{\alpha}\frac{\partial\vartheta}{\partial\zeta} \qquad (10)$$

With μ and α the fluid dynamic viscosity and thermal diffusivity and p the pressure. The axial variation of the fluid temperature along the channel can be deduced from an energy balance

$$\frac{\partial\vartheta}{\partial\zeta}=\frac{\partial\vartheta_b}{\partial\zeta}=\frac{q_{wall}}{\rho c_p W\Omega} \qquad (11)$$

where θ_b is the fluid bulk temperature, ρ its density, q_{wall} the heat flux at the heated walls and W the bulk fluid velocity.

Introducing the non-dimensional quantities:

$$x=\frac{\xi}{D_h}\quad y=\frac{\eta}{D_h}\quad z=\frac{\zeta}{D_h}\quad \Gamma^*=\frac{\Gamma}{D_h}\quad \Omega^*=\frac{\Omega}{{D_h}^2}\quad \nabla^*=D_h\nabla$$

$$V(x,y)=\frac{u}{W}\quad z=\frac{\zeta}{D_h}\quad p^*=\frac{{D_h}^2}{\mu W}\frac{dp}{d\zeta}\quad T=\frac{\lambda(\theta-\theta_{in})}{q_{wall}}$$

Equations (1) and (2) can be rearranged to read:

$$\nabla^{*2}V=-p^* \qquad (12)$$

$$\nabla^{*2}T=\frac{V(x,y)}{\Omega^*} \qquad (13)$$

While boundary conditions for the cases investigated become

$$V|_{\Gamma^*}=0\quad \frac{\partial T}{\partial y}\Big|_{\Gamma^*_u}=0\quad T|_{\Gamma^*-\Gamma^*_u}=0 \qquad (14)$$

The first equality expresses the no-slip

condition for velocity, whereas the second and third represent the adiabatic condition at the unheated perimeter (Γ^*_u) and the imposed temperature at the heated length; depending on the cases investigated the unheated perimeter's length may be zero.

From the solutions of (9) and (10), which yield the velocity and temperature fields, the Poiseuille and local Nusselt numbers can be obtained. For the former

$$\mathrm{Po}=\mathrm{fRe}=\frac{1}{2\Omega^*}\int_{\Omega^*}\nabla^*\cdot\left(\nabla^*\mathrm{V}\right)\mathrm{d}\Omega^* \quad (15)$$

where f is the Fanning friction factor and Re the Reynolds number. For the latter

$$\mathrm{Nu}_l=-\frac{1}{\mathrm{T_b}}\left(\mathbf{n}\cdot\nabla^*\mathrm{T}|_{\mathrm{wall}}\right) \quad (16)$$

with **n** the unity vector normal to the wall and T_b the nondimensional bulk temperature, defined as:

$$\mathrm{T_b}=\frac{1}{\Omega^*}\int_{\Omega^*}\mathrm{V(x,y)T(x,y)}\mathrm{d}\Omega^* \quad (17)$$

Integration of (16) yields the average Nusselt number, Nu, for the cross-section.

For the rectangular geometry, the cases studied are those of H1 boundary conditions, with either all sides heated or one short side adiabatic, the latter being the case for microchannels covered by an adiabatic sealing lid. In the former configuration, all corners are rounded, whereas in the latter only the corners of the heated short side are modified.

For the trapezoidal cross-section, the only case studied was that with three sides heated uniformly with imposed temperature and the longest side adiabatic. Again, only the corners of the shorter side were rounded.

The solutions have been computed through a code written with the commercial solver FlexPDE 5.0.19 using a normal desktop PC.

This package solves systems of partial differential equations through a Rayleigh-Ritz-Galerkin finite element method. The numerical procedure evolves through an iterative refinement of the grid until the prescribed accuracy, related to the maximum local residual value, R_k, is reached.

The iterative procedure is stopped when the velocity field *V* and the temperature field *T* satisfy the inequality

$$\max\left(\mathrm{R_k(V,N)},\mathrm{R_k(T,N)}\right)<\varepsilon\ \forall k\in[1,N] \quad (18)$$

In order to obtain satisfactory accuracy while keeping computational time to a minimum, the average Nusselt numbers obtained by computation, Nu_{cal}, have been compared to those available for reference cases, Nu_{th}. Table I reports the results for a square microchannel under H1 boundary conditions and all sides heated. The same procedure has been followed for the friction factor.

Table I – Values of Nu as a function of ε

ε	Nu_{cal}	Nu_{th}	$\Delta Nu_{\%}$
10^{-1}	3.619591	3.60795	0.322
10^{-2}	3.619583	3.60795	0.322
10^{-3}	3.619594	3.60795	0.322
10^{-4}	3.61399	3.60795	0.167
10^{-5}	3.611078	3.60795	0.086
10^{-6}	3.608405	3.60795	0.012
10^{-7}	3.608042	3.60795	0.002

As a satisfactory compromise, the value of $\varepsilon=10^{-6}$ has been chosen. For the case of trapezoidal microchannels, the results for sharp corners and different values of β were compared to those available in the literature (Shah and London, 1978, Morini and Spiga, 2007), with discrepancies at most of the order of 10^{-4}.

2. Results and discussion

Simulations were run holding the aspect ratio fixed and varying the radius of curvature. As the non-dimensional form of the latter parameter is bounded by the value of β or γ, the number of cases investigated varies with the aspect ratio. The runs yield numerical outputs and graphical plots of the quantities of interest (velocity and temperature fields) and of the ones which can be derived, e.g. the local Nusselt number. The results for the latter are also depicted for the same case in Fig. 3.

The variation of Nu along the length of the perimeter can readily be appreciated, as well as its symmetric distribution

As a first step, cases analogous to those present in the literature have been computed

for comparison purposes.

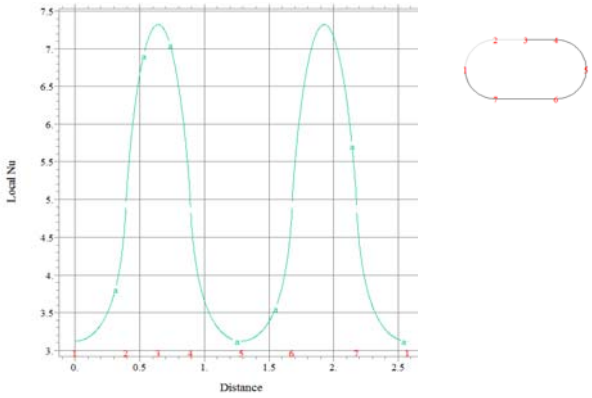

Figure 3 – Nusselt number distribution for β=0.5, R_c^*=0.5

Figure 4 shows the calculated results for the Poiseuille (circles) and Nusselt (squares) numbers and compares them to the correlations given by Ray, Misra and Laha, 2002 for the case of a square cross-section (β=1), as the nondimensional radius of curvature varies, namely

$$Po=fRe=14.226\left[1+\sum_{k=1}^{5} B_k R_c^{*k}\right] \quad (19)$$

and

$$Nu=3.608\left[1+\sum_{k=1}^{5} A_k R_c^{*k}\right] \quad (20)$$

whose coefficients are reported in Table II.

Table II Coefficients for Eq. (19) and (20)

Index i	**A_i**	**B_i**
1	0.4316	0.4258
2	-0.5549	-0.00903
3	0.2067	-0.7139
4	0.1451	0.7976
5	-0.1040	-0.2909

As can be seen the agreement is excellent, and the limiting values of Po and Nu for the cases of square and circular duct (the result for β=1 and R_c^*=1).

Some further data available in literature (Shah and London, 1978) for stadium-shaped ducts of nondimensional radius of curvature equal to the channel's aspect ratio and H1 boundary conditions were also compared with the corresponding calculations and the agreement was more than satisfactory. For the case of three heated sides, the comparison was made with the results of Morini, 2007, for rectangular and trapezoidal ducts with sharp corners, with and without viscous dissipation. The agreement with data used for reference was complete.

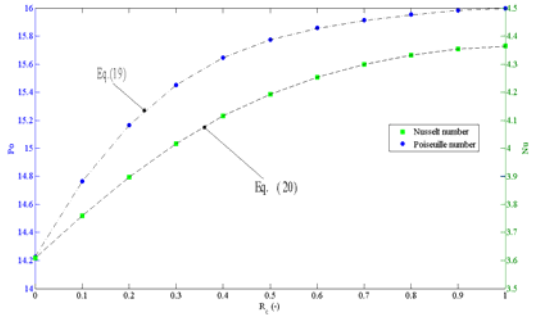

Figure 4 – Poiseuille and Nusselt numbers for β=1 as a function of R_c^* and comparison with Eqs. (19), (20).

2.1 Rectangular cross-section, four sides heated

Five different aspect ratios were investigated: β=1, β=0.50, β=0.25, β=0.10, β=0.03 for different values of R_c^*.

The Poiseuille number and average Nusselt number were calculated, and equations relating them to the nondimensional radius of curvature were obtained. The results for Po and Nu are shown in Tables III to VII.

Table III – Values of Po and Nu for β=1

R_c^*	**Po**	**Nu**
0.0	14.226	3.609
0.1	14.765	3.759
0.2	15.167	3.898
0.3	15.452	4.017
0.4	15.646	4.115
0.5	15.775	4.193
0.6	15.858	4.253
0.7	15.914	4.298
0.8	15.954	4.332
0.9	15.985	4.355
1.0	15.999	4.366

Table IV – Values of Po and Nu for β=0.50

R_c^*	**Po**	**Nu**
0.00	15.548	4.124
0.05	15.952	4.239
0.10	16.278	4.348
0.20	16.725	4.530
0.30	16.964	4.654
0.40	17.055	4.714
0.50	17.027	4,709

Table V – Values of Po and Nu for β=0.25

R_c^*	Po	Nu
0	18.232	5.331
0.03	18.572	5.438
0.05	18.759	5.505
0.10	19.108	5.649
0.15	19.317	5.749
0.20	19.415	5.800
0.25	19.412	5.795

Table VI – Values of Po and Nu for β=0.10

R_c^*	Po	Nu
0.00	21.168	6.787
0.01	21.321	6.840
0.02	21.450	6.888
0.03	21.556	6.932
0.04	21.643	6.971
0.05	21.713	7.006
0.06	21.767	7.032
0.07	21.807	7.053
0.08	21.834	7.066
0.09	21.850	7.073
0.10	21.851	7.073

Table VII – Values of Po and Nu for β=0.03

R_c^*	Po	Nu
0	23.058	7.751
0.01	23.206	7.809
0.02	23.281	7.845
0.03	23.306	7.858

For each aspect ratio, correlations were given that fit the Nusselt and Poiseuille numbers as functions of the nondimensional radius of curvature. The correlations have the form

$$\mathrm{Po}=\sum_{k=0}^{4} C_k R_c^{*k} \quad (21)$$

and

$$\mathrm{Nu}=\sum_{k=0}^{3} D_k R_c^{*k} \quad (22)$$

with the corresponding coefficients reported in Table VIII and IX. As can be clearly seen from the tabular results, the Nusselt number increases with the value of the nondimensional radius of curvature, as does the Poiseuille number. This is easily explained if one considers that at the corners the fluid stagnates when they are sharp, and thus the frictional resistance drops, while convective heat transfer is modest, whereas smoothing the corners increases the local flow velocity and engenders an increase in convective heat transfer and frictional resistance.

Table VIII– Values of coefficients for Eq. (21)

β	C_3	C_2	C_1	C_0
0.50	9.3319	-16.303	8.7752	15.5506
0.25	35.2394	-39.2648	12.3279	18.2346
0.10	263.986	-120.85	16.2793	21.1691
0.03	0	-307.5	17.415	23.0591

Table IX – Values of coefficients for Eq. (22)

β	D_3	D_2	D_1	D_0
0.50	-1.2969	-1.9492	2.4705	4.1225
0.25	-11.342	-4.8322	3.774	5.3303
0.10	-72.067	-19.178	5.4948	6.7868
0.03	0	-112.5	6.945	7.7509

It is to be noticed that both parameters increase with aspect ratio, but the enhancement due to rounded corners is less and less pronounced as β decreases. The case giving the highest increases is that of β=1; it is evident from both the values in Table III as well as the graphical representation of Fig. 4 that the rate of increase in Nu is higher at low values of R_c^* and is comparatively small for R_c^*>0.5. The maximum increase of Nu and Po are 21% and 12% respectively for β=1, R_c^*=1 (corresponding to a circular duct) and drops to 9% and 6% for β=0.25, R_c^*=0.25; this is also readily explained considering that as the aspect ratio decreases the role of the rounded corners loses in influence on the global behaviour of the channel.

2.2 Rectangular cross-section, three sides heated

When only three sides are heated (the fourth being adiabatic, 3L,S), the temperature profile modifies as in Fig. 5.

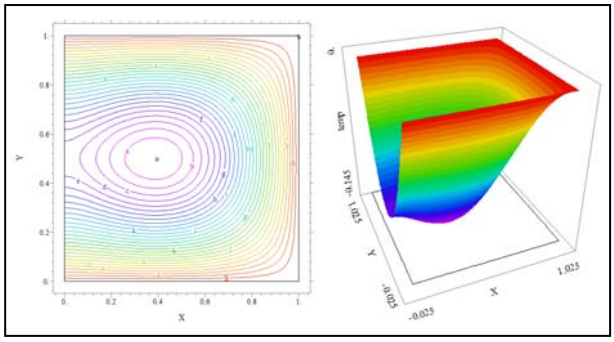

Figure 5 – Temperature profile, case β=1, 3L,S

Runs were carried out for the same values of β as before and the results are reported in Table X to XIV. Again, the rounding of the corners

brings an increase in both Nusselt and Poiseuille numbers, but it is far more moderate that for the case of four sides heated, and ranges from 10% and 5% respectively at β=1 to less than 1% for β=0.03.

Table X – Values of Po and Nu for β=1, 3L,S

R_c^*	**Po**	**Nu**
0.0	14.223	3.572
0.1	14.489	3.657
0.2	14.682	3.735
0.3	14.811	3.802
0.4	14.895	3.857
0.5	14.946	3.898
0.6	14.976	3.926
0.7	14.996	3.943
0.8	15.010	3.950
0.9	15.023	3.949
1.0	15.036	3.938

Table XI – Values of Po and Nu for β=0.5 3L,S

R_c^*	**Po**	**Nu**
0.00	15.548	4.539
0.05	15.748	4.609
0.10	15.905	4.674
0.20	16.113	4.781
0.30	16.216	4.851
0.40	16.247	4.884
0.50	16.223	4.876

Table XII – Values of Po and Nu for β=0.25 3L,S

R_c^*	**Po**	**Nu**
0.0	18.232	5.760
0.05	18.492	5.860
0.10	18.660	5.939
0.15	18.756	5.995
0.20	18.798	6.023
0.25	18.791	6.022

Table XIII – Values of Po and Nu for β=0.1 3L,S

R_c^*	Po	Nu
0.00	21.168	7.048
0.01	21.244	7.075
0.02	21.308	7.101
0.03	21.360	7.124
0.04	21.403	7.145
0.05	21.436	7.163
0.06	21.463	7.177
0.07	21.482	7.187
0.08	21.494	7.195
0.09	21.501	7.198
0.10	21.501	7.198

The coefficients to be introduced in Eq. (21) and (22) are reported in Tables XV and XVI.

Table XIV – Values of Po and Nu for β=0.03 3L,S

R_c^*	**Po**	**Nu**
0	23.058	7.845
0.01	23.132	7.876
0.02	23.169	7.894
0.03	23.181	7.900

Table XV– Values of coefficients for Eq. (21), 3L,S

β	**C_4**	**C_3**	**C_2**	**C_1**	**C_0**
1.00	-0.9237	3.5142	-4.9225	3.146	14.222
0.50	- 5.4108	10.670	10.273	4.496	15.548
0.25		19.926	-20.608	6.143	18.2325
0.10		137.918	-61.515	8.104	21.1686
0.03			-155.00	8.710	23.0586

Table XVI– Values of coefficients for Eq. (22), 3L,S

β	**D_3**	**D_2**	**D_1**	**D_0**
1.00	0.05614	-0.6548	0.96583	3.5697
0.50	-0.63204	- 1.334	1.4999	4.5383
0.25	-4.0741	-3.5365	2.1865	5.76
0.10	-39.4328	-9.9592	2.8909	7.0476
0.03	-	-62.50	3.705	7.845

2.3 Trapezoidal cross-section, three sides heated

For the trapezoidal cross-section, the only case investigated was that of three sides heated. The aspect ratio has no upper limit (β=∞ corresponds to a triangular shape), and thus simulations have been run for 20 different values of β. An example of temperature profile in the cross-section is shown in Fig. 6.
For the trapezoidal cross-section, the parameter γ, defined in section 2, substitutes the nondimensional radius of curvature.

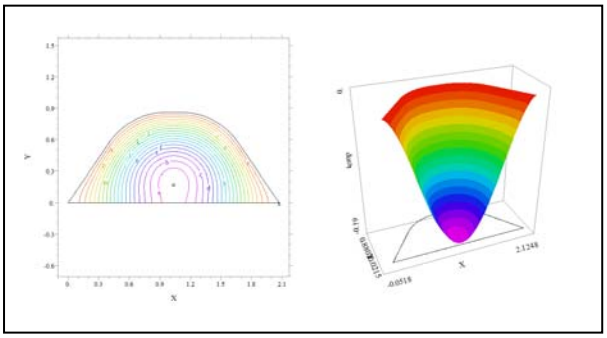

Figure 6 – Temperature profile, case β=1, 3L,S

For this kind of geometry, where only the corners on the shortest side are rounded, there is very little increase in the values of the Poiseuille and Nusselt numbers.

This is readily explained considering the geometries in Fig. 7: for values of β below unity, the sides where heat transfer takes place are mainly the two bases, and the smoothing of the corners only affects a negligibly small length compared to the heated perimeter, whereas when β becomes greater than unity, the geometry tends toward a triangular shape, where the rounding of only one vertex again little influences the heat transfer and frictional characteristics of the duct.

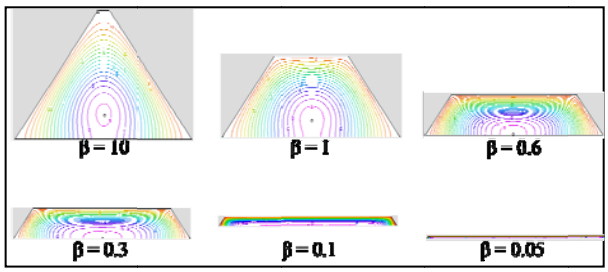

Figure 7 – Aspect ratios for trapezoidal cross-sections.

The maximum increase should then be thought to take place around β=1, which is in fact confirmed by the data reported in Table XVII. The maximum increase occurs for the upper middle values of γ (0.7-0.8), but is very moderate (2.4 % and 1.5% for the Nusselt and Poiseuile numbers respectively), so under the aforementioned conditions the results for sharp edges (Morini and Spiga, 2007) can still be used. For the same reason, no polynomial correlation in the form of Eq. (21), (22) are given for the trapezoidal geometry.

Table XVII– Values of Po and Nu for β=1

γ	Po	Nu
0.00	14.063	2.884
0.10	14.125	2.904
0.20	14.162	2.920
0.30	14.188	2.932
0.40	14.208	2.940
0.50	14.225	2.946
0.60	14.244	2.950
0.70	14.266	2.952
0.80	14.293	2.952
0.90	14.325	2.951
0.95	14.342	2.951
1.0	14.110	2.852

As a last remark, it is to be noticed that the values of Nu and Po drop although the absolute value of the decrease is moderate. A possible explanation for this is the disappearance of the straight portion of the shortest side.

3. Conclusions

Fully-developed laminar flow in microchannels under H1 boundary conditions has been investigated for rectangular and trapezoidal cross-sections with rounded corners, when all or three sides heated. The Poiseuille and Nusselt numbers have been calculated and correlations given to link them to the nondimensional radius of curvature.
Smoothing of the corners invariably results in an improvement, which is more marked for the rectangular sections, with a maximum for β=1 when all sides are heated. The enhancement decreases with the aspect ratio, and also for the case when only three sides are heated. For the trapezoidal cross sections, maximum enhancement is at about β=1, but is around 2% at best, so edges can be treated as sharp.

4. References

Collins, M., Karayiannis, T., Rosa, P. 2008 Review of heat transfer in microchannels, Proc. 1st European Conf. on Microfluidics, Bologna 10-12 Dec.
Laha G., Misra, D., Ray, S., 2002 Pressure Drop and Heat Transfer Characteristics of Laminar Flow Through Ducts of Square and Triangular Cross Sections with Rounded Corners, Proceedings of 5th ASME-ISHMT, Kolkata, 341 – 346.
London A. L., Shah, R.K., 1978, Laminar flow forced convection in ducts Adv. In Heat Transfer, Academic Press, 274
Morini, G.L., 2004, Single-phase convective heat transfer in microchannels: a review of experimental results, International Journal of Thermal Sciences, 43, 631-651.
Morini, G.L., Spiga, M., 2007, The Role of the Viscous Dissipation in Heated Microchannels ASME J heat Transfer, 129, 308-318.
Pal, P., Sato, K., 2009, Various Shapes of Silicon Freestanding Microfluidic Channels and Microstructures in one-step Lithography, J. Micromech. Microeng., 19, 05 5003.